International Journal of Fatigue 210 (2026) 109692

Contents lists available at ScienceDirect

International Journal of Fatigue

journal homepage: www.elsevier.com/locate/ijfatigue

Effective stress determination for flat bars with sharp notches by combining the theory of critical distances with artificial neural networks

Kane F. ter Veer [a,b], Mathis Harder [a], Kagan Koyunseven [b], Sascha M. Isay [b], Moritz Braun [a,b,*]

[a] German Aerospace Center (DLR), Institute of Maritime Technologies and Propulsion Systems, Düneberger Str. 108, D-21502 Geesthacht, Germany
[b] Hamburg University of Technology, Institute of Ship Structural Design and Analysis, Am Schwarzenberg-Campus 4C, D-21073 Hamburg, Germany

ARTICLE INFO

Keywords:
Notch fatigue
Fracture mechanics
Stress gradient
Metamodeling
Artificial neural network
Surrogate modelling

ABSTRACT

This work systematically quantifies the deviations of gradient methods from the Theory of Critical Distances (TCD) and introduces neural-network-based metamodels for the rapid prediction of effective stresses in notched flat bars. Stress-based fatigue and fracture assessment methods often rely on the local stress field around a notch and are commonly referred to as effective stress or stress-gradient methods. In this study, notched flat bars are examined as a representative structural detail. The influence of geometrical variation, critical distance, loading, and plane state on the resulting effective stresses is investigated using the point, line, and area methods of TCD. Deviations of up to 40% are identified across certain geometry–loading combinations, highlighting the sensitivity of TCD based assessment to parameter variations. To eliminate the need for a dedicated numerical simulation for every new notch geometry, a series of feedforward artificial neural network (ANN) metamodels is developed and trained on thousands of finite element simulations. Particular attention is given to the effect of optimization algorithms on training performance and predictive robustness. The resulting metamodels provide fast and accurate estimates of effective stresses across a wide range of geometries and loading conditions, offering a computationally efficient alternative to repeated finite element analysis for the assessment of notched components.

1. Introduction

It is well known that material failure through fatigue or brittle fracture often initiates at notches, where localized stress and strain concentrations occur. Consequently, the consideration of notches plays a crucial role in engineering design. Fatigue or fracture strength at notches is understood to be governed not by its peak elastic stresses, rather by its surrounding stress field [1]. The reason for this is the micro-structural support effect at notches, which is influenced by high stress field gradients, the local plastic zone at the notch root, and initial damage in the form of microscopic cracks [2].

Several stress-based approaches exist for calculating the fatigue and fracture strength of structures and components with notches. The theory of critical distances (TCD) is a group of gradient methods used to predict notch failures with consideration of the elastic stress field with respect to critical material stress and distance constants [2]. Typical applications are assessment of machined components [3–8], welded [9–17] or adhesion joints [18–20], but also rock mechanics [21,22], additively manufactured components [23,24], cut-edges [25,26], or cavities such as pores [27,28] or pitting corrosion [29,30]. TCD encompasses four methods: point, line, area, and volume [2]; however, previous comparisons have shown that the effective stresses determined by different variants of the TCD may differ [17,31–36]. This will lead to variations in prognosed fatigue life or fracture toughness. The deviations caused by using different stress gradient methods have not yet been systematically investigated for notched components under various loadings, stress methods and plane states.

A new or adjusted numerical simulation—typically with finite element analysis (FEA)—is required for each individual notch geometry, making the process computationally expensive and time-consuming. Metamodeling offers the possibility to determine effective stresses by creating a surrogate that is trained using a large number of FEA results. Similar approaches utilizing neural networks have recently been presented to determine stress concentration factors in welded joints [37–41]; however, there are no such approaches for stress gradient

* Corresponding author at: German Aerospace Center (DLR), Institute of Maritime Technologies and Propulsion Systems, Düneberger Str. 108, D-21502 Geesthacht, Germany.
E-mail address: moritz.braun@dlr.de (M. Braun).

https://doi.org/10.1016/j.ijfatigue.2026.109692
Received 14 January 2026; Received in revised form 24 March 2026; Accepted 16 April 2026
Available online 17 April 2026

Nomenclature

TCD	Theory of critical distances
ANN	Feedforward neural network
FEA	Finite element analysis
MSE	Mean squared error
PM	Point method
LM	Line method
AM	Area method
d	Notch depth [mm]
r	Notch radius [mm]
ω	Notch opening angle [°]
h	Flat bar height [mm]
r_{AM}	Radius of the semi-circle area for AM calculation [mm]
r_{PM}	Distance used in PM calculation [mm]
r_{LM}	Stress averaging length for LM [mm]
s	Polar coordinate distance originating from notch root [mm]
θ	Polar coordinate angle [°]
σ_{eff}	Effective stress [MPa]
σ_0	Critical stress [MPa]
σ_n	Nominal stress. In this study constant of 1 MPa
M_{nom}	Nominal moment used in bending load case [Nmm]
L	Material characteristic length [mm]
C	Load case as tensile to bending factor
$D_{1,2}$	Effective stress deviation [%]
$q_{1,2}$	Conversion ratio for gradient methods
n	FEA elements along 360° curve
K_c	Critical stress intensity for brittle fracture (fracture toughness)
ΔK_{th}	Fatigue crack propagation threshold
$\Delta\sigma_0$	Fatigue limit of plain specimens
$\boldsymbol{\phi}_i$	Pre-activation layer response
$\boldsymbol{x}_{gain}$	Gain vectors for ANN prediction model input normalization
$\boldsymbol{x}_{offset}$	Offset vectors for ANN prediction model input normalization
$\boldsymbol{y}_{gain}$	Gain vectors for ANN prediction model output normalization
$\boldsymbol{y}_{offset}$	Offset vectors for ANN prediction model output normalization
$\boldsymbol{W}$	Weight matrices
$\boldsymbol{b}$	Bias matrices
$\boldsymbol{x}$	Input layer matrix for neural network
$\boldsymbol{y}$	Output layer matrix for neural network

methods for notched components yet.

This study thus:

- quantifies deviations caused by different TCD variants to improve the comparability of different effective stress methods, and
- explores the use of metamodels and proposes a workflow for fast effective stress calculations at notched flat bars based on artificial neural networks (ANNs).

For these purposes, thousands of numerical simulations were performed for flat bars with varying notch geometry. From the FEA results, effective stresses are determined for each of the different calculation methods belonging to the TCD. Feedforward ANNs are trained using the resulting datasets to create three metamodels: a model for first principal stresses, a model for von Mises stresses under plane stress, and a model for von Mises stresses under plane strain. Particular attention was given to the selection and evaluation of training optimizers, as the accuracy and convergence behavior of ANN-based surrogates can vary substantially depending on the optimization algorithm used with respect to the dataset [42,43]. In this study, both first- and second-order optimization methods are assessed to ensure that the metamodels are trained appropriately. Combinations of notch geometry parameters, loading case, and the material characteristic length can then be input directly into the metamodels to determine effective stress values, enabling rapid predictions without the need for FEA or stress field integration.

2. Stress gradient methods

The fatigue strength of a material, according to the effective notch stress approach, is not specified by either peak stress σ_{max} or nominal stress σ_{nom}. Instead, it is determined by the effective stress σ_{eff}. Various methods exist for determining the effective stress. The TCD, proposed by Taylor [2] whilst building on the works of Peterson [44] and Neuber [1], encompasses a group of methods using the common feature characteristic material length parameter—sometimes also referred to as critical distance—L. Here the main aim of TCD is to simplify predictions for fatigue failure and brittle fracture for notched specimens, where the elastic stress field around the stress concentration feature is known. Although the relationships used in TCD were originally derived analytically for a sharp crack in an infinite plate under tension [45], the approach is now commonly extended to notches by evaluating the local elastic stress field around the notch root [2].

In this study, three of the TCD methods are considered: the point, line and area methods, see Fig. 1. Each of these methods aims to describe how the critical stress σ_0 and characteristic material length can be used to predict the loading at which failure will occur. However, the results of evaluating the stress-distance curve vary depending on the TCD method used [36].

The effective stress this can be expressed for each of the methods as:

$$\sigma_{eff,PM} = \sigma\left(\frac{L}{2}\right) \tag{1}$$

$$\sigma_{eff,LM} = \frac{1}{2L}\int_0^{2L} \sigma(s, \theta = 0)ds \tag{2}$$

$$\sigma_{eff,AM} = \frac{4}{2\pi}\int_{-\frac{\pi}{2}}^{\frac{\pi}{2}}\int_0^{r_{AM}=1.32L} \sigma(s,\theta)dsd\theta \tag{3}$$

Each of the TCD methods is linked through a factor applied to the material characteristic length .i.e. $\frac{L}{2}$, $2L$ and $1.32L$ which are argued to be valid for the case of a simple notched specimen [2,17]. The material characteristic length L, in turn, can be defined for static problems [34] as:

$$L_s = \frac{1}{\pi}\left(\frac{K_c}{\sigma_0}\right)^2 \tag{4}$$

This expression defines the relationship between the fracture toughness K_c and the material constants of the TCD. When assessing fatigue strength, the same equation is able to be used by replacing the static parameters with cyclic parameters.

$$L_c = \frac{1}{\pi}\left(\frac{\Delta K_{th}}{\Delta\sigma_0}\right)^2 \tag{5}$$

Assessing fatigue strength, it can be shown based on fracture mechanics that L_c is related to the fatigue crack propagation threshold ΔK_{th} and the fatigue limit of plain specimens $\Delta\sigma_0$. It is worth noting, however, that ΔK_{th} and $\Delta\sigma_0$, and consequently L_c depend not only on the material,

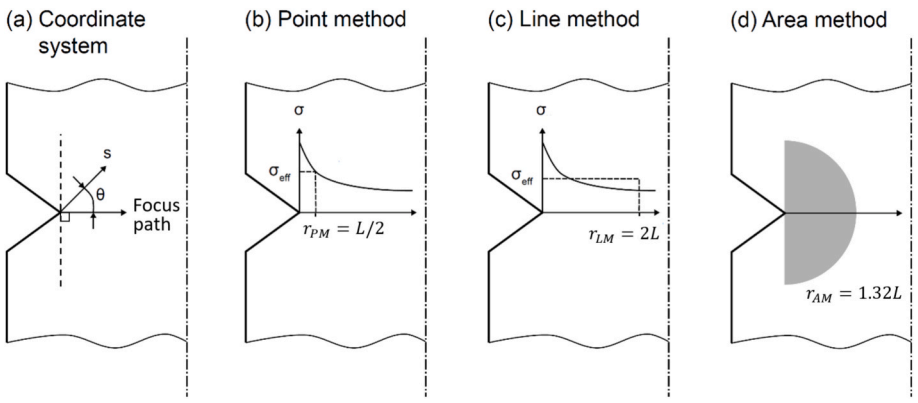

Fig. 1. Point, line and area methods for the stress gradient calculations. Adapted from Susmel and Taylor [46].

but also on the stress ratio and the number of cycles until failure [2,47]. Thus, varying L_c values for the same material may emerge from high-cycle or medium-cycle fatigue regimes [34].

3. Parametric study on notched flat bars

3.1. Finite element model

A notched flat bar (see Fig. 2) was chosen for this study as it is one of the most frequent notch details and extensively studied in literature, c.f., [33,47–54]. The finite element model used for the analysis builds on the related work by Braun *et al.* [36], in which a symmetrical notched specimen was simulated with variable geometric parameters. While analytical solutions for idealized notched geometries may represent an alternative approach to estimate the notch stresses prior to the effective stress determination, the use of FEA in this study allows the effective stress for all three applied TCD methods to be derived from the same geometry-specific stress field without requiring separate derivations, which is particularly advantageous for the two-dimensional stress field integration required for the AM evaluation. The three main input parameters in this study—notch depth d, notch radius r, and the notch angle ω—are incrementally varied for each unique combination within the defined parameter value ranges, see Table 1.

The remaining geometric parameters for the flat bar length and section height are set as constants throughout the simulations. A mesh sensitivity study was performed previously for the model in [36], where it was found that 32 elements over a full circle with quadratic shape function were found to be sufficient to achieve a stress error of less than 1%. In this study, 144 elements over a full circle are used, as n = 32 failed to converge for the geometries with small notch depths. Furthermore, using a finer mesh around the notch root allows for more datapoints near the notch root in the nodal stress solution, which is critical location when comparing the gradient methods.

Table 1
Ranges for the geometric notch parameters used in the FEA models.

Geometric parameter	Range	Increment	Variations
Notch depth d	1.5 –5mm	0.5 mm	8
Notch radius r	0.1 –0.8 mm	0.05 mm	15
Opening angle ω	0° –140°	10°	15

In addition to a simple nominal tensile loading, bending is applied to investigate the influence of different load cases on the effective stresses. This bending is applied as a moment through a pilot node, evenly distributing the moment across all nodes on the edge surface. The magnitude of M_{nom} is set so the maximum stress from bending on the unnotched geometry at the upper edge is equal to the nominal stress from tensile loading. Superposition is then applied to obtain mixed tensile and bending loadings.

The commercial software ANSYS® is used to programmatically run the simulations, in which scripts containing each of the input parameter combinations are run through the Mechanical APDL client through the PyMAPDL library [55] in Python. A total of 7200 two dimensional FEA simulations are run. This includes 1800 unique geometrical combinations, along with bending and pure tension load cases, evaluated under both plane stress and plane strain states. Introducing a thickness effect under plane stress was investigated in the FEA simulations; however, this was found to have no influence on the resulting effective stresses for the simulated geometry parameters. The element type used is PLANE183 with nominal isotropic material values of 200 GPa for elastic modulus and 0.3 for Poisson's ratio. The sensitivity of the results to Poisson's ratio was additionally evaluated, where the range of 0.25 – 0.35 led to a

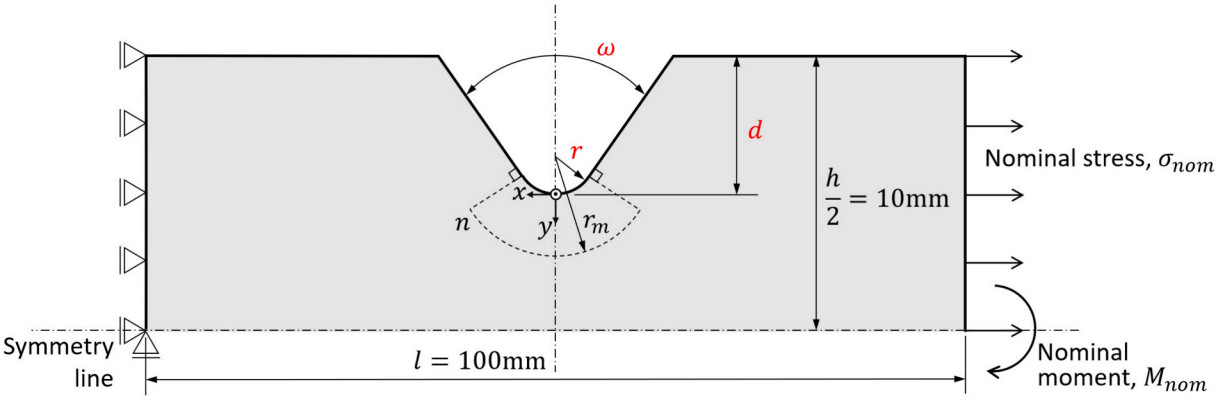

Fig. 2. Geometry and load parameters for the notched specimen.

variation of approximately ±1.5% in maximum von Mises stress with plane strain state. The variation was negligible in all other stress methods and plane state combinations.

3.2. Effective stress determination

Using the elastic stress field results from the FEA simulations, Python scripts were implemented to identify relevant nodes for each of the gradient methods and calculate the effective stresses according to each of the TCD methodologies.

The value of the material characteristic length L is applied to all three methods as a range between 0 - 1.5 mm which includes values for most common metallic materials with the notable exception of cast irons [46,56]. The effective stress for each of the three TCD methods is then calculated for each iteration of L. The most extreme gradient shifts in effective stress are known to occur near the notch root [36]; thus, to reduce computational load, finer iterations are used at decreasing L values, as shown in Table 2. Due to the underlying spacing of mesh nodes in the FEA analysis, an iteration larger than 0.01 mm would not increase the accuracy of the stress results.

For the PM and LM calculations, the FEA determined stresses are only considered at nodes located on the focus path [2]. Nodal stress values are then used to construct a piecewise cubic Hermite interpolating polynomial, enabling accurate estimation of stresses at locations between the FEA nodes. The PM and LM effective stresses are then evaluated at respective critical distances r_{PM} and r_{LM} for each iteration of L.

On the other hand, the area method requires the evaluation of the stress field in a semicircle originating at the notch root. To this aim, nodal stresses from the FEA stress field are interpolated over a 2D uniform grid using a piecewise Clough-Tocher cubic interpolation scheme, see Fig. 3. To determine the effective stresses, the interpolated grid of stresses is then integrated with double composite trapezoidal through a semicircular mask of radius $r_{AM} = 1.32L$ for each L iteration.

As one would expect given the gradient function equations, the effective stresses from PM, LM and AM converge to the maximum stress concentration factor at the notch root as the characteristic material length L approaches 0. To illustrate the differences between the stress gradient methods, deviation percentages are calculated for the effective stress results. In line with statistical theory, this is determined with the deviation percentage D, such that:

$$D_{1,2} = 100 \bullet \frac{\sigma_{eff,1} - \sigma_{eff,2}}{\sigma_{eff,2}} \, [\%] \tag{6}$$

Furthermore, it is already known from the literature that the suggested ratios applied to L for each of the TCD methods are $r_{PM} = \frac{L}{2}, r_{LM} = 2L$ and $r_{AM} = 1.32L$ for PM, LM, and AM, respectively [2]. In the recent study by Braun *et al.* [36], the ratios with respect to PM and LM are analyzed comparatively through a conversion factor q, where:

$$q = \frac{r_{PM}}{r_{LM}} \tag{7}$$

The value for q is then determined for which the equation $\sigma_{eff,PM} = \sigma_{eff,LM}$ is satisfied, such that

Table 2
Range of material characteristic length L used in the effective stress calculations.

L range [mm]	Iteration [mm]
0 – 0.05	0.01
0.05 – 0.2	0.025
0.2 – 0.5	0.05
0.5 – 0.7	0.1
0.7 – 1.0	0.15
1.0 – 1.5	0.5

$$\sigma_{eff,PM}(L) = \sigma_{eff,LM}(q \bullet L) \tag{8}$$

The equivalence equation is then solved to determine q. Given the aforementioned ratios, a value of $q = 0.25$ would indicate the PM and LM methods produce the same effective stress for a given material characteristic length. For this study, however, three different TCD methods are considered. We therefore expand the approach by assuming one of the gradient methods as a reference. For this, PM is chosen as it is the simplest of the three methods and most commonly applied in practical fatigue and fracture assessments. This is then represented by

$$\sigma_{eff,\mathrm{PM}}(r_{PM}) = \sigma_{eff,m}\left(q_{PM,m} \bullet r_m\right), \tag{9}$$

where $m \in \{\mathrm{LM}, \mathrm{AM}\}$. Here, the gradient method dependent critical distance r_m already has the ratios from L applied. This increases the interpretability of the q factor, where a value of 1 would indicate the gradient methods give the equivalent effective stress for a given material characteristic length and stress field. By determining this conversion factor, we are able to systematically evaluate the ratios of L for the TCD gradient methods for different parameters and loadings.

4. Metamodeling with feedforward ANNs

A multilayer perceptron (MLP) is a type of feedforward fully connected artificial neural network well suited for creating regression models in engineering contexts, see [37–40]. The model creates a nonlinear mapping from an input vector $\boldsymbol{x}$ to an output $\boldsymbol{y}$ through a sequence of transformations and activation functions [57]. This consists of an input layer, several hidden layers with nonlinear activation functions, followed by the output layer, see Fig. 10. Each hidden layer first computes an affine transformation of the previous layer output by multiplying it with the weight matrix $\boldsymbol{W}$ and adding the bias vector $\boldsymbol{b}$. The resulting pre-activation response $\boldsymbol{\phi}$ is then passed through the layers activation function f to calculate the activation $\boldsymbol{a}$.

For each feature $j = 1, \cdots, n_0$ in the input vector, pre-activation response is determined with

$$\boldsymbol{\phi}_{1j} = \boldsymbol{b}_{1j} + \sum_{k=1}^{n_0} \boldsymbol{W}_{1jk} \boldsymbol{x}_k. \tag{10}$$

The activation for each neuron in the following layer is then determined by

$$\boldsymbol{a}_{1j} = f_1\left(\boldsymbol{\phi}_{1j}\right) \quad for \quad j = 1, \cdots, n_1 \tag{11}$$

This algorithm is then repeated for the hidden layers $\ell = 2, \cdots, N-1$, where N is the total number of layers. This is expressed for each hidden layer by

$$\boldsymbol{\phi}_{\ell j} = \boldsymbol{b}_{\ell j} + \sum_{k=1}^{n_{\ell-1}} \boldsymbol{W}_{\ell jk} \boldsymbol{a}_{\ell-1,k}, \tag{12}$$

followed by the activation:

$$\boldsymbol{a}_{\ell j} = f_\ell\left(\boldsymbol{\phi}_{\ell j}\right) \text{ for } j = 1, \cdots, n_\ell \tag{13}$$

Finally, the output vector y from the final layer N for the neural network is calculated by

$$\boldsymbol{y}_j = \boldsymbol{b}_{Nj} + \sum_{k=1}^{n_{N-1}} \boldsymbol{W}_{Njk} \boldsymbol{a}_{N-1,k}, \tag{14}$$

with $j = 1, \cdots, n_N$.

4.1. Training the neural network

Training a feedforward neural network involves iteratively adjusting its weights and biases to minimize a chosen loss function, typically by following the gradient of the error. Optimization algorithms used for this purpose can be broadly classified into first-order and second-order methods, and the choice of optimizer plays a crucial role in the models performance [42,43]. First-order optimizers, such as gradient

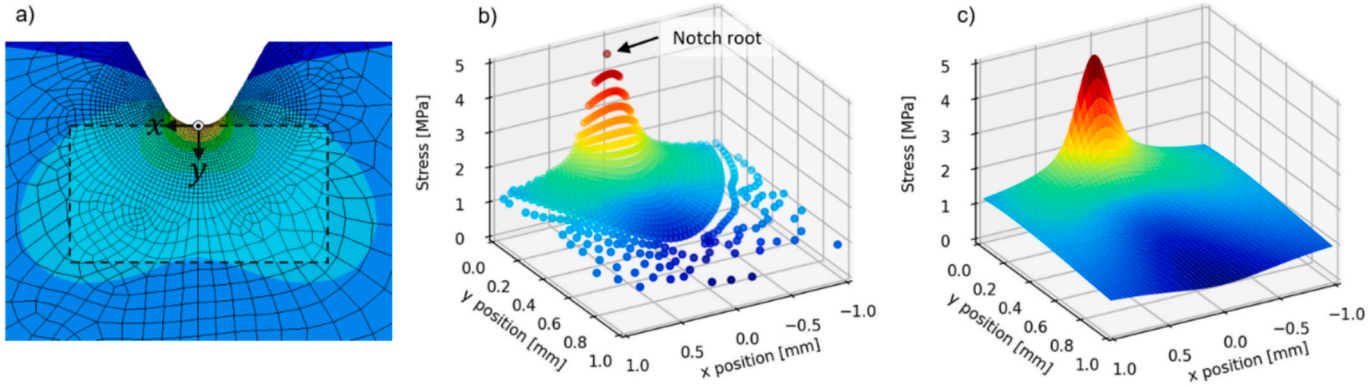

Fig. 3. Von Mises stress field results under bending load from geometric parameters $d = 1.5\text{mm}, r = 0.40\text{mm}$ and $, \omega = 60^{\circ}$ under plane strain showing a) nodal stress field from FEA solution. b) uniform grid of stress field using piecewise cubic interpolation of nodal results.

descent variants and the commonly used Adam, rely exclusively on gradient information to determine the update direction. They are computationally efficient and scale well to large datasets, but their convergence can be slow or unstable when the loss surface is highly curved [58]. Second-order methods, in contrast, use information about the curvature of the loss function through approximations of the Hessian matrix to make more informed updates. This often results in faster convergence and improved accuracy [58,59], especially for smaller to medium-sized networks. However, second-order techniques generally require more memory and computational effort, which limits their applicability to large or deep neural networks. From the aforementioned literature [42,43,58,59], there is a lack of consensus on which optimization method is best suited for training an ANN for specific regression related application or dataset. Thus, both first- and second-order optimization functions are investigated in this work.

For the first-order optimization, the popular opensource TensorFlow Python library is used. The three optimizers ADAM, RMSprop and stochastic gradient decent are tested during hyperparameter tuning. Here the best performance is achieved using the ADAM optimizer with a learning rate of 0.01. The best performing architecture is a network with 2 hidden layers both with 56 neurons and rectified linear units (ReLU) activation functions. To avoid overfitting early stopping with a patience of 10 epochs is applied.

For the second-order optimization, The MATLAB® *Deep Learning Toolbox* is utilized to train the model with the Levenberg-Marquardt backpropagation algorithm, known to be well suited to regression problems [58]. Using hyperparameter tuning, an architecture of 3 hidden layers of 10 neurons was found to perform well with hyperbolic tangent sigmoid (tansig) activation functions for the hidden layers. During training, a mean squared error (MSE) value of 5×10^{-5} is chosen as a target loss function with maximum number of epochs set at 1000. Additionally, the minimum momentum gradient ν_{min} of the loss function during training is set at 10^{-6}. These training parameters help control the convergence of the learning algorithm and ensure that the training process stops within the defined constraints.

For training, the dataset is split to 70% training, 15% testing, and 15% validation. To increase the stability while training, the feature vector $\boldsymbol{x}_f$ from the training data is normalized to the range $-1 < x < 1$ before entering the network. this is done through the *mapminmax* function, which is defined by

$$\boldsymbol{x} = \left(\boldsymbol{x}_f - \boldsymbol{x}_{offset}\right) \bullet \boldsymbol{x}_{gain} - 1 \tag{15}$$

The inverse is also applied to the output vector $\boldsymbol{y}$ to obtain the effective stress predictions, with

$$\boldsymbol{\sigma}_{eff,ANN} = \frac{\boldsymbol{y} + 1}{\boldsymbol{y}_{gain,out}} + \boldsymbol{y}_{offset,out} \tag{16}$$

Identical data splits and normalization procedures are used for both the MATLAB and TensorFlow training data to reduce bias and standardize the comparison of the optimization methods. Once the weights, biases, and normalization parameters are obtained following training, the MLP becomes a fixed mathematical function that can be evaluated independently of the software used to generate the model. Thus, the model parameters are exported from MATLAB and TensorFlow after training and reapplied using a lightweight script for the effective stress predictions.

In addition to training with the raw FEA simulation data, percentage-based noise was added to the targets to simulate a dataset with experimental error. The objective here is to compare how the optimization methodologies perform with controlled scatter. The targets with added noise are generated through

$$\widetilde{\boldsymbol{\sigma}}_{eff,FEA} = \boldsymbol{\sigma}_{eff,FEA} \bullet (1 + p\varepsilon) \tag{17}$$

Here, ε represents a normally distributed random variable with mean of 0 and standard deviation of 1 and p is the noise factor. For instance, an addition on 10% noise equates to $p = 0.1$.

5. Results

Each FEA simulation including geometry creation and meshing took an average of 5.7 seconds to complete using a consumer grade workstation. The FEA results for first principal stresses are the same when applied with plane stress and plane strain element behavior. As such, only the results for von Mises stresses are differentiated between plane strain and plane stress analysis, see Fig. 4. The different combinations of loading cases, stress methods, and element behaviours clearly have a significant effect on the stress contours of the elastic stress field, and thus the resulting stress gradients. Each of the stress fields was evaluted across the 23 iterations of L for first principal and von Mises stresses individually to determine the stress gradients for each of the TCD methods.

5.1. Gradient method deviations

After determining the effective stresses, a comparative study was conducted to evaluate the results of the TCD methods. Overall, the TCD methods showed substantial variation in deviations across the parameter combinations, indicating different error levels in fatigue or fracture predictions. LM was generally seen to be the most conservative of the three methods, while the PM usually resulted in the highest effective stress. Exceptions were found however, for example the notch geometry shown in Fig. 5.a evaluated under bending with plane strain. Here, using the PM indeed results in the highest effective stress for lower L values, with a result 29.1% higher than the other methods for L = 0.05 mm. At L

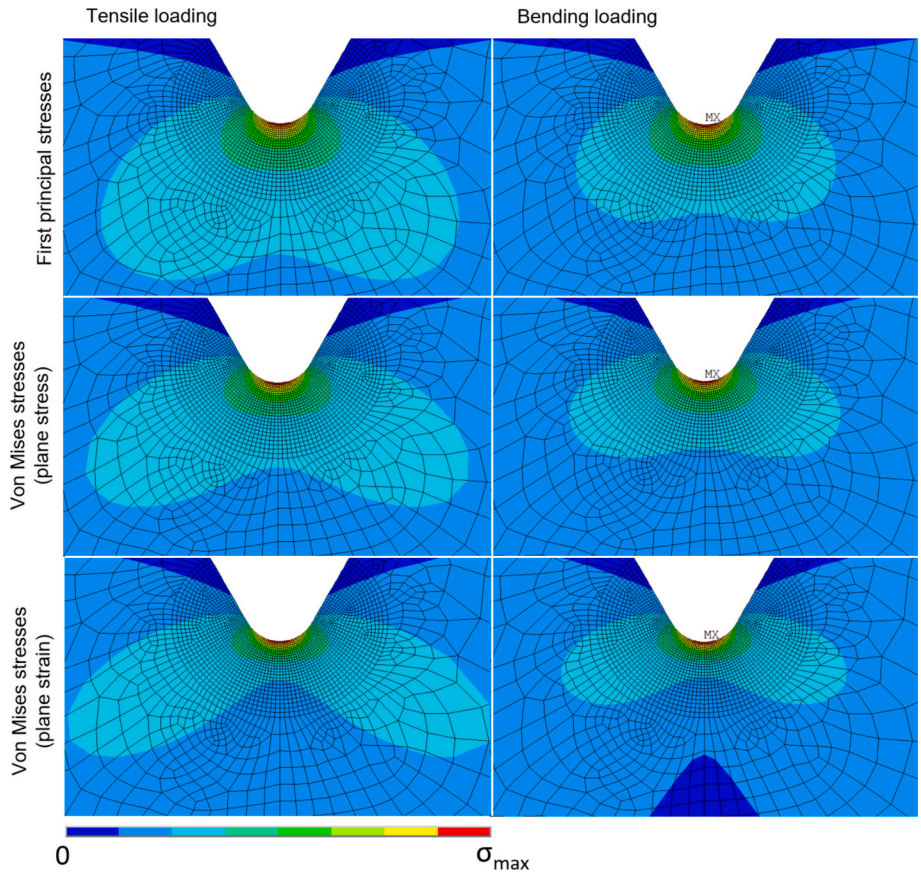

Fig. 4. Normalized stress field results as matrix for different load cases and stress methods as contour diagrams for $d = 2.0$mm, $r = 0.40$mm and $\omega = 60^{\circ}$ with plane stress and plane strain element behaviors.

$= 1.5$ mm on the other hand, the effective stress from PM was the most conservative with a value 40% lower than that of the other methods, with this trend seen to continue for L > 1.5 mm. This geometry coincides with the highest absolute effective stresses calculated across the study, with both the smallest notch radius, smallest opening angle, and largest notch depth of all the simulated parameter sets. This additionally shows that the sharpest notch geometries tend to result in larger deviations between the TCD methods.

Looking strictly at the first principal stresses, the highest deviation was also seen with largest notch depth and no opening angle; however, the maximum notch radius of $r = 0.8$mm resulted in the largest deviation of 24.2% under bending load, see Fig. 5.b This deviation diverges out at the maximum $D_{PM,LM}$ at the upper range of $L = 1.5$mm. Under tension loading the maximum deviation is seen at approximately $L = 0.5$mm for $D_{PM,LM}$.

Deviations calculated under bending tended to be larger and more sensitive to geometric variation than those under tension, also tending to diverge for larger L values as seen in Fig. 5 for both plane strain and plane stress. This suggests that the TCD conversion factors may be poorly suited for bending loading and evaluations under plane strain. Deviations in von Mises stresses for plane strain were generally the highest in the dataset and similarly showed strong sensitivity to geometric parameters. Figs. 6–8 further show how the individual geometrical parameters d, r, and ω influence the effective stress results across different loading cases, element behaviors and stress methods. Changes in notch depth d are seen to have the smallest effect on the deviation percentages, with only a few percentiles difference observed within the range of $1.5\text{mm} \leq d \leq 5\text{mm}$ for both tensile and bending loading, see Fig. 7. The notch radius r on the other hand is seen to have the largest influence of deviations between the gradient methods, especially with larger L values. The opening angle showed mixed results, with its effect on the deviations changing depending on other aspects of the geometry, shown for different notch radii in Fig. 6.

5.1.1. Conversion factors

For the determination of conversion factors one of the gradient methods is used as a reference point, at which the two other gradient methods are compared to determine the conversion factor q for which the effective stress from both methods is equal. For this study, AM is chosen as the reference as it is seen to represent the median result of the three methods across the majority of parameter combinations. As such, the assumption is made that $r_{AM} = 1.32L$ holds true and the following q values are calculated with the conditions for the PM and LM being respectively satisfied as defined in (9). Diagrams illustrating the effect of the different geometrical parameters, loading cases, element behaviors and stress methods on the conversion factor q can be found in Fig. 9. Interestingly, the conversion factors show poor equivalency at small L values, where most convergence is seen at larger L values and smaller notch radius. Furthermore, bending load cases and analysis with von Mises under plane strain show relatively low equivalency. This suggests the given ratios may be unsuitable for such scenarios due to the clear instability between the TCD methods.

5.2. ANN-based metamodels

Using the datasets from the gradient method results, ANN-based metamodels were trained to predict effective stresses based on first principal and on von Mises stresses under both plane strain and plane stress conditions, resulting in three independent neural networks with the same feature vector for the input layer, see Fig. 10. Separate models using first principal stress results under plane strain and plane stress are not required as the effective stresses through these methods are equal.

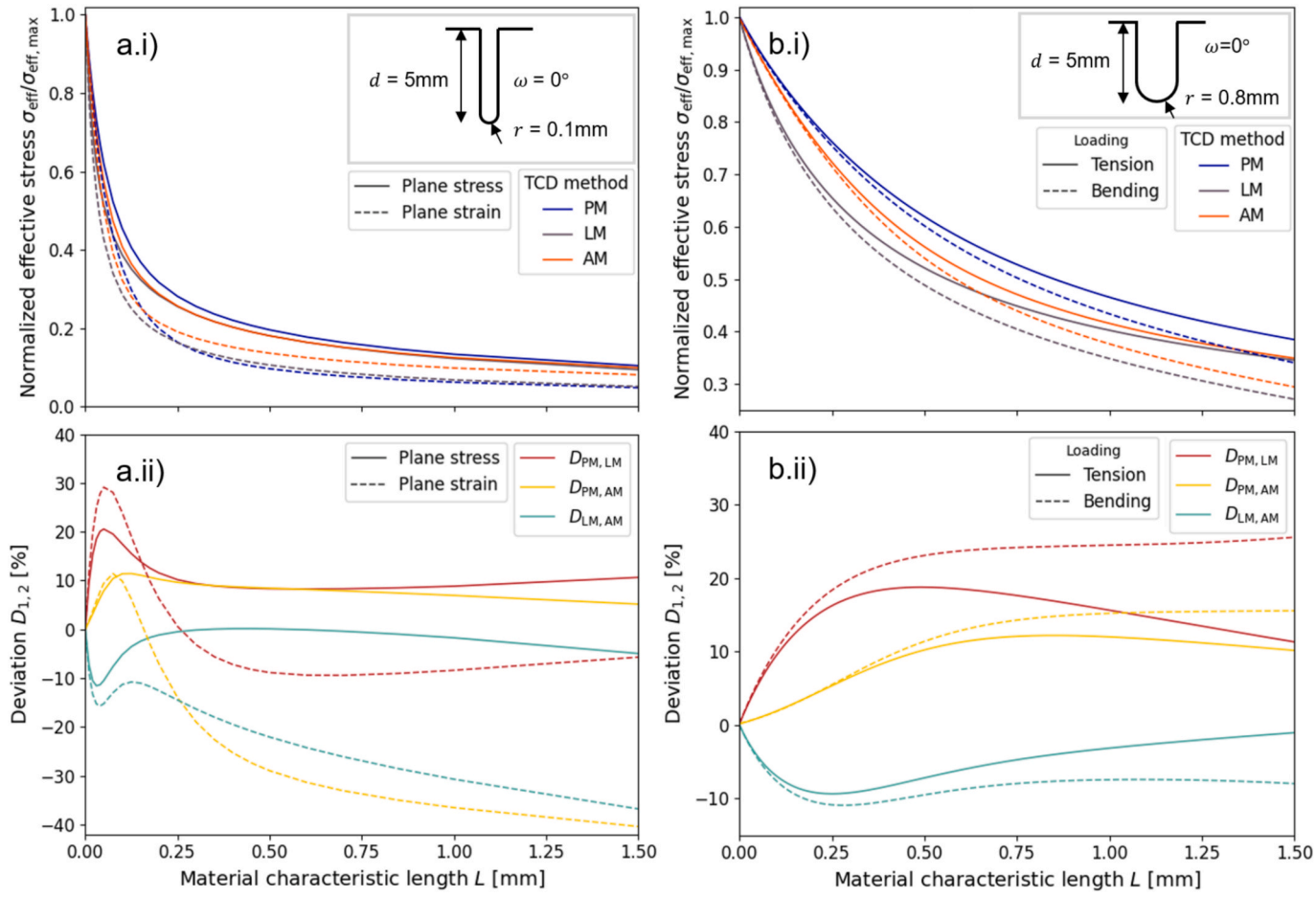

Fig. 5. Comparing the normalized effective stresses (top) and deviation percentages (bottom) for each of the TCD methods for: a) bending loading with von Mises stresses and 0.1mm radius notch comparing plane stress and plane strain and b) first principal stresses with 0.8mm radius notch comparing bending and tensile loadings. The normalizations and deviations are calculated independently for each plane state and loading type.

The input features include the notch-geometry parameters, the material characteristic length, and a loading-case scalar ranging from 0 (pure tension) to 1 (pure bending). This scalar is incorporated into the training data through superposition of the tensile and bending FEA results at six evenly spaced intervals between these loading conditions. The targets for the ANNs are the effective stress results for each of the three respective gradient methods. Considering the ranges for the parameters d, r, ω, L and the superposed loading case C, a total of 248,400 distinct parameter combinations form the raw dataset for each of the three metamodels.

For the models trained with the second-order Levenberg-Marquardt optimization, the target MSE of 5×10^{-5} was achived in validation for all three models reliably under 1000 Epochs. The time taken for each model to achieve the training target was an average of under 20 minutes with a consumer grade workstation. For the first-order Adam optimization on the other hand, a validation MSE of between 3×10^{-3} and 5×10^{-3} was achieved before training ended after early stopping. The training with Adam was marginally faster, averaging approximately 15 minutes.

Interestingly, the 2nd order optimization Levenberg-Marquardt gave substantially better results for both R^2 and MSE metrics. The training performance for each model can be seen in Fig. 11. The final MSE values for the individual gradient methods after training for both Levenberg-Marquardt and Adam optimization is shown in Table 3 for the testing dataset. Fig. 12 shows a direct comparison of the resulting residuals between the ANNs trained with Adam and Levenberg-Marquardt for each of the three models. Interestingly, the predictions from the Adam-trained models tend to become unstable for higher effective stresses, whereas Levenberg-Marquardt has relatively stable absolute residuals across the target domain.

The resulting trained ANNs are able to predict the results for the three TCD effective stresses for over a hundred thousand parameter-sets in under a second when implemented through a lightweight script, many multitudes faster than the hours needed to do the same with FEA followed by stress field interpolation and integration.

Fig. 13 shows the residuals from the three trained metamodels with respect to each of the notch parameters. Here the raw dataset is are subtracted from the ANN predictions and plotted as colourmaps for each TCD method and geometrical parameter. For each geometrical parameter, the other features are set to defaults where the largest absolute residuals are seen to occur. This corresponds to $d = 5.0$ mm, $r = 0.1$ mm and $\omega = 140°$ with pure bending loading case. It can be seen in the colormaps that the largest absolute residuals commonly occur at the edges of the feature domain. This is commonly seen at max and min values for L, but also at the max and minimum geometrical parameters, especially r and ω. This is unsurprising, as neural-network metamodels typically give reduced accuracy near the boundaries of the training domain, where fewer data combinations exist and the models rely more heavily on extrapolative behavior.

Noise was also added to the FEA target variables to investigate the effects this had on the performance of the optimization methods. To this goal, a new model was trained using the first principal stress-based dataset in which 10% randomly distributed gaussian noise was added to the target variables. The results for a single notch geometry subset are shown in Fig. 14. Here, the discreet points for the effective stresses from

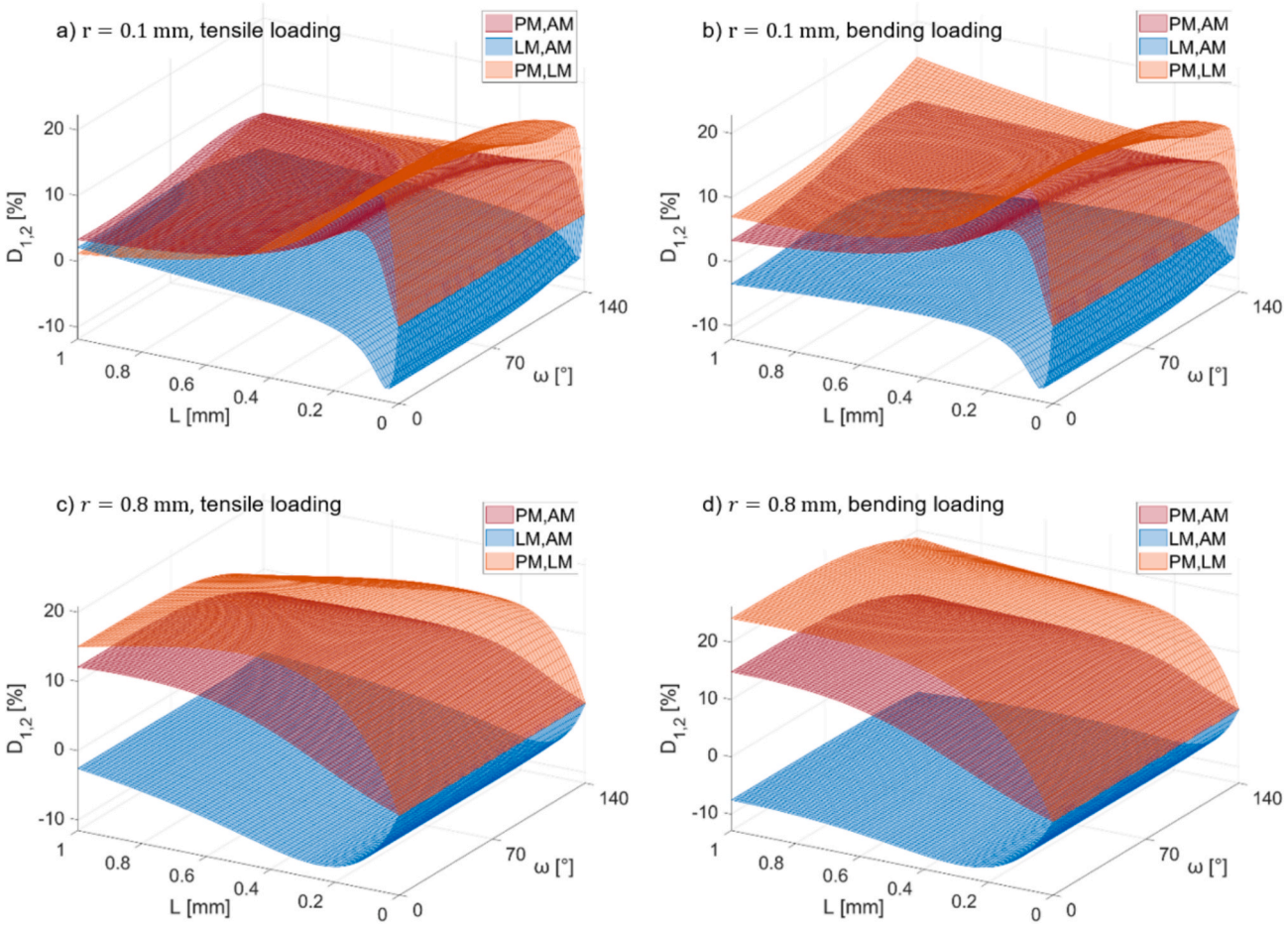

Fig. 6. Deviations in effective stress with first principal stresses across different opening angles with $d = 5$mm for tensile and bending load cases.

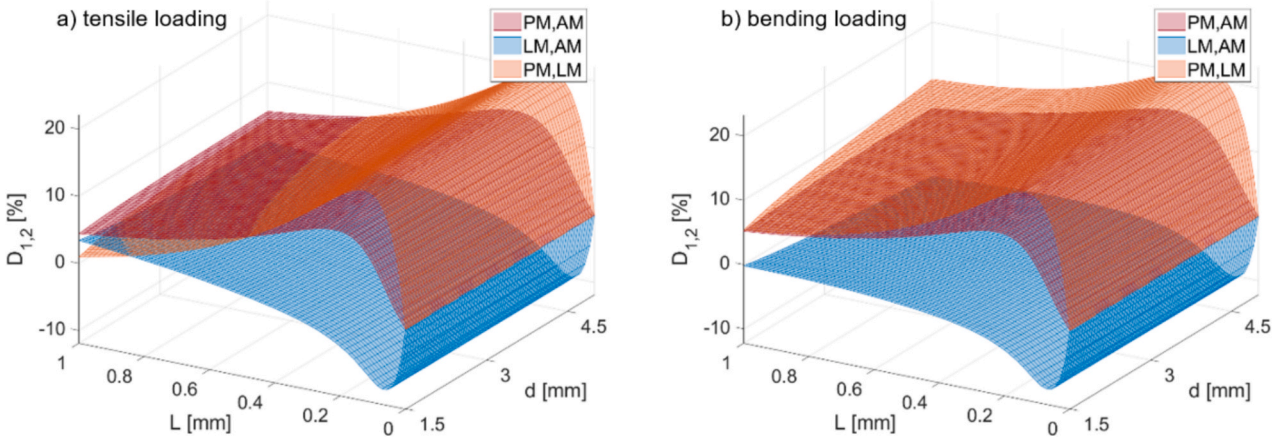

Fig. 7. Deviations in effective stress calculations with first principal stresses across different notch depths with $r = 0.2$mm, $\omega = 20^{\circ}$.

the FEA simulations are shown both with and without 10% added noise. The predicted effective stresses are evaluated at iterations of 0.01mm between $0 < L < 1.5$ mm, which includes predictions between the discreet points in the FEA simulations. This indicates how well the ANN predictions follow the trend of the data, in which a smooth contour was observed without signs of stepping or overfitting. The MSE and R^2 metrics are additionally shown for the ANN in relation to the raw targets and those with noise. While the ANNs trained on the raw dataset unsurprisingly achieved better MSE values in training, the ANN trained here with scatter was seen to follow the underlying data trends closely for all three TCD methods.

6. Discussion

The premise that notch failure is governed by a finite physical zone surrounding the notch, rather than the maximum stress at the notch root, is well established in the literature. Nevertheless, numerous studies have shown that geometry and loading conditions strongly influence the deviations between the individual TCD methods, with changes in notch sharpness or loading mode producing substantial differences in their

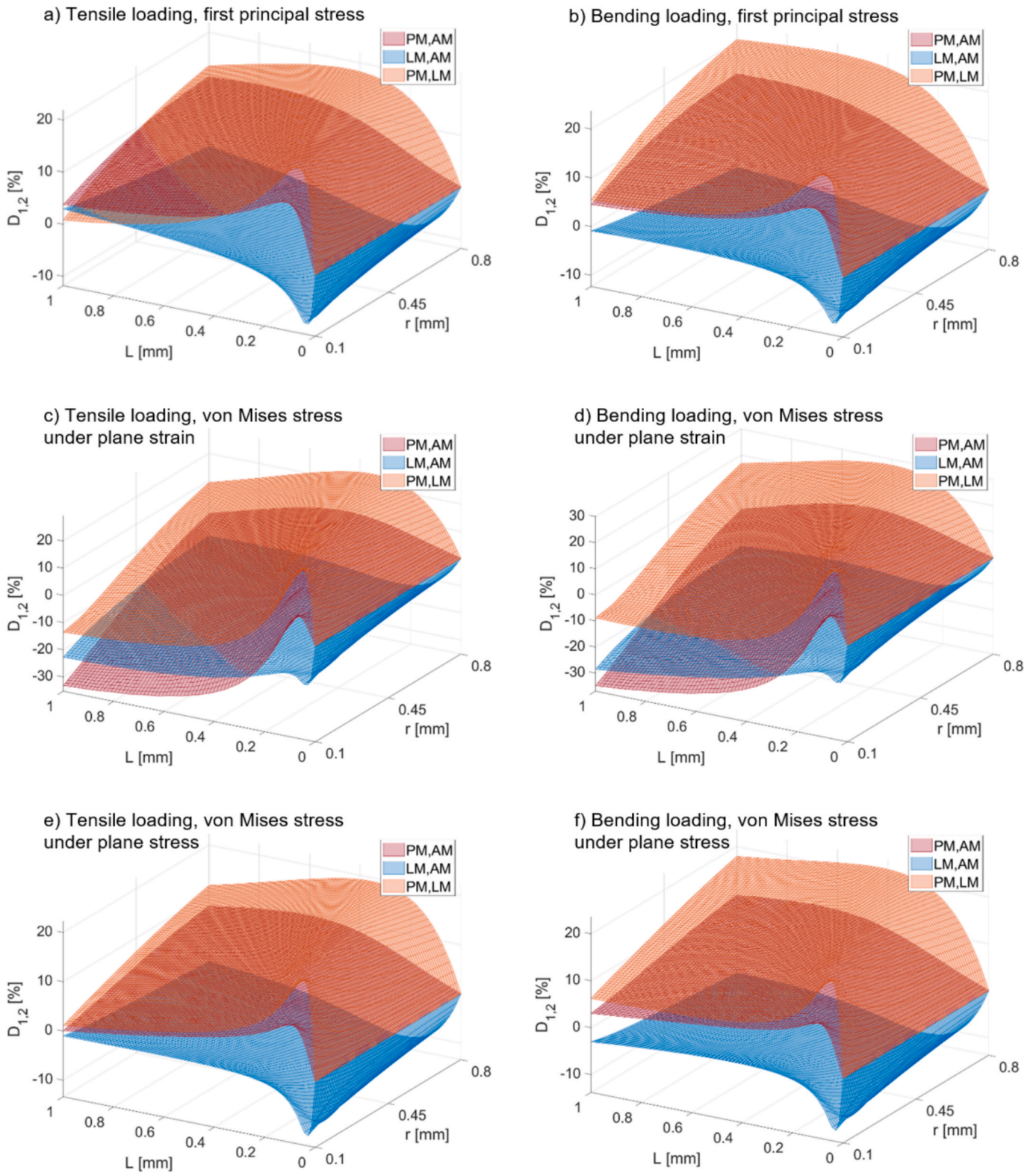

Fig. 8. Diagrams showing effective stress deviations under different loadings, element behavior and stress method for different notch radii with $d = 3\text{mm}, \omega = 60^{\circ}$.

predicted effective stresses [2,4,34,36,56]. The overall maximum deviations determined in our work were $|D_{PM,AM}| = 40.4\%$ and $|D_{PM,LM}| = 24.2\%$ under bending for von Mises and first principal stress methods, respectively. When only considering PM and LM under tension, the values were somewhat less at $|D_{PM,LM}| = 28.4\%$ for von Mises and $|D_{PM,LM}| = 20.3\%$ for first principal. This is comparable to the 27.5% value for von Mises stresses [36] under plane strain and 20% determined for first principal in related studies [36,46]. The trends obtained in our work are interesting, as there has been little prior research systematically comparing deviations of TCD methods under different loading cases and plane states, shown in this paper to have a significant effect on the deviations. Furthermore, 20% variation in effective stresses applied to a fixed slope S-N curve was found to result in over 100% difference in

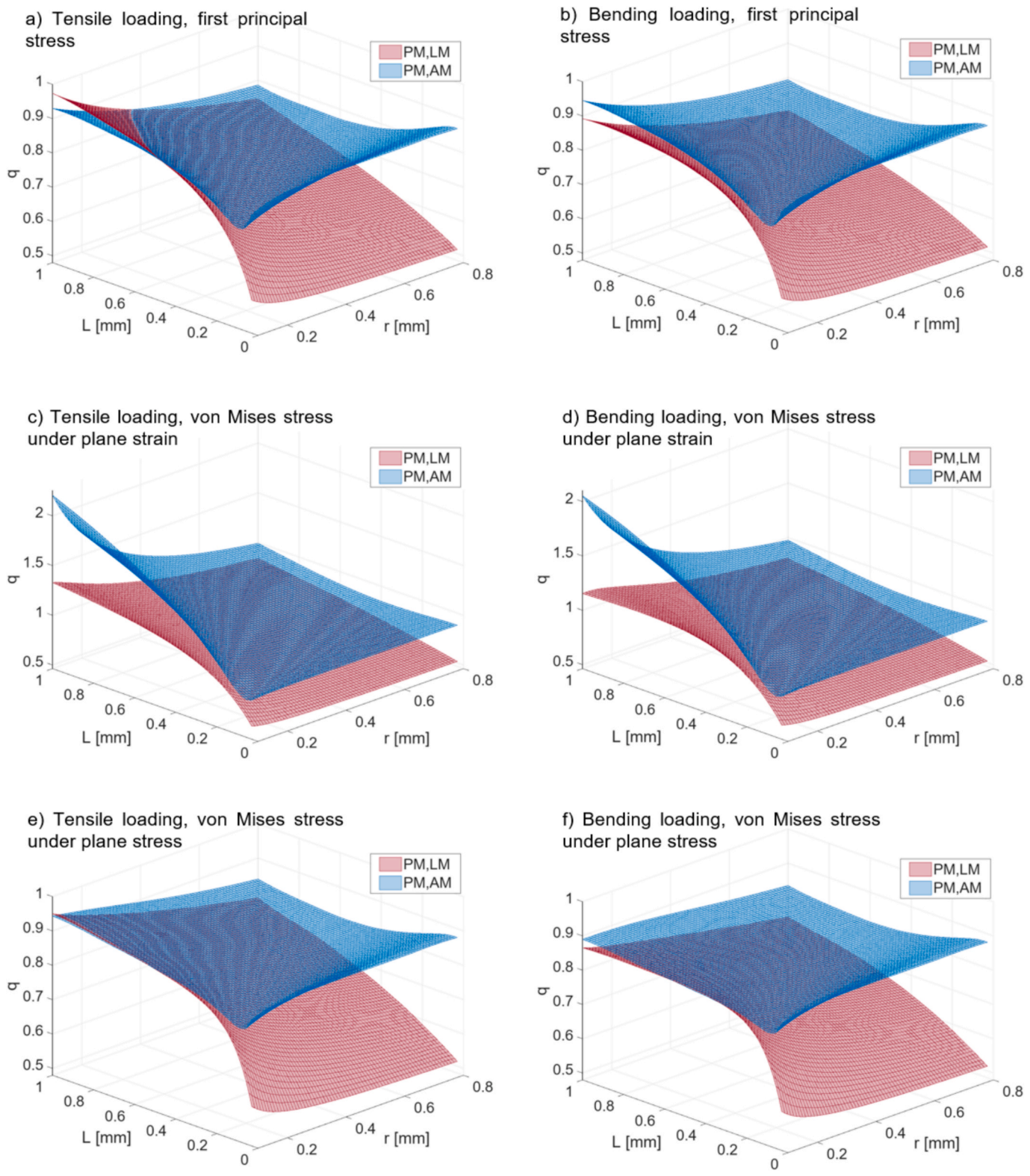

Fig. 9. Gradient method conversion factors under different loading cases, element behavior and stress method for different notch radii with $d = 5\text{mm}, \omega = 0^{\circ}$.

predicted fatigue life for welded joints, see Baumgärtner et al. [10]. The variations seen in this work are substantially more, leading to the question of applicability of the TCD methods within certain specimens and load scenarios. The conversion factor q, gives insight on how the critical distance may be adjusted between methods to ensure an equal effective stress [36]. This ratio is determined to be highly dependent on both geometry and plane state, see Fig. 9. Thus, although it gives an effective visualization of trends within the parameter sets where the conversion factors between the TCD methods are seen to diverge or converge, using q to provide an improved ratio between methods is subjective and not able to be generalized to such a parameter set.

The original analytical derivations of the TCD were developed for a sharp crack in an infinite plate under tensile loading [45], whereas the present study considers notches with finite root radii and determines the

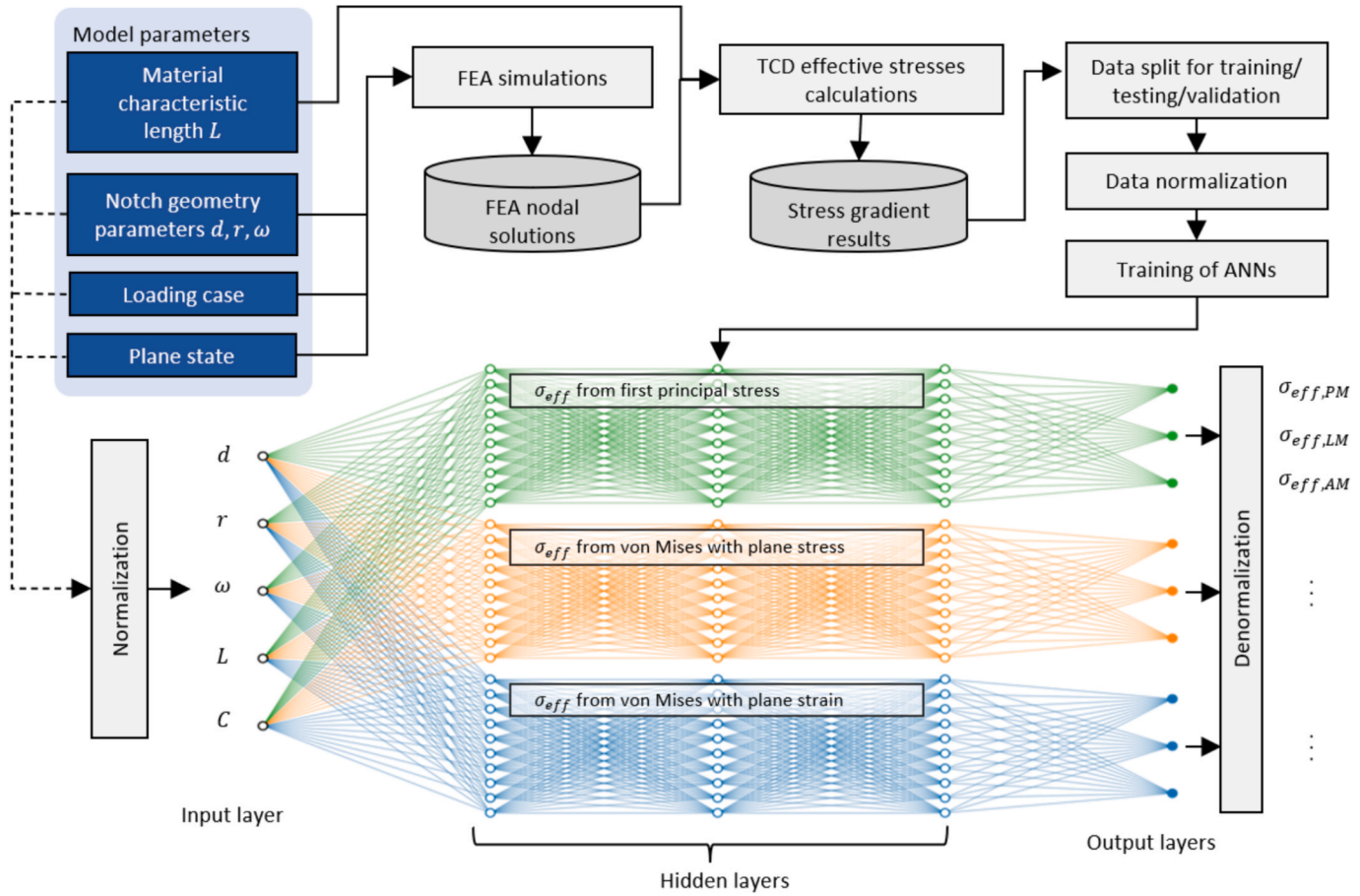

Fig. 10. Visual representation of the ANN networks using three hidden layers with 10 neurons per layer.

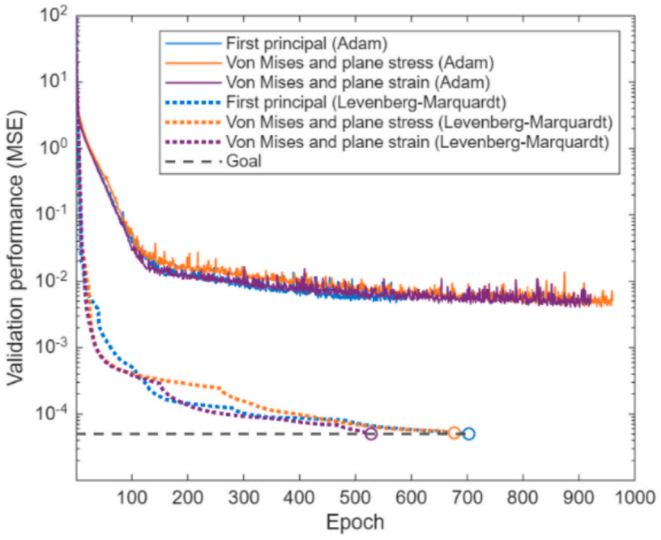

Fig. 11. Training performance showing the loss function based on the validation dataset for each of the metamodels.

elastic stress fields with FEA. This aligns with the observation that the use of the maximum principal stress under tensile loading leads to improved agreement between the TCD methods, as it directly represents the Mode I crack-opening stress governing fatigue initiation in the original theoretical framework. In contrast, von Mises stress under plane strain includes an additional out-of-plane stress component due to Poisson constraint, which is not considered in the 2D evaluation of

Table 3
Resulting validation metric for different metamodels and gradient methods.

Stress and plane method	TCD method	Test MSE (Levenberg-Marquardt)	Test MSE (Adam)
First principal stresses	PM	5.24×10^{-5}	3.27×10^{-3}
	LM	4.79×10^{-5}	6.68×10^{-3}
	AM	4.93×10^{-5}	3.58×10^{-3}
Von Mises under plane stress	PM	5.03×10^{-5}	2.97×10^{-3}
	LM	4.59×10^{-5}	4.95×10^{-3}
	AM	5.46×10^{-5}	3.31×10^{-3}
Von Mises under plane strain	PM	4.74×10^{-5}	3.34×10^{-3}
	LM	4.38×10^{-5}	5.58×10^{-3}
	AM	6.31×10^{-5}	3.67×10^{-3}

maximum principal stress or in von Mises stress under plane stress conditions. This likely explains why resulting trends based on von Mises (plane stress) and maximum principal stress are similar, while under plane strain the deviations follow markedly different trends with larger deviations between the TCD methods (see Figs. 8–9). Nevertheless, the TCD has been successfully applied using the von Mises stress criterion under multiaxial loading, as demonstrated by Susmel and Taylor [60], and Baumgärtner et al. [10] reported a reduction in scatter of welded joint S–N data when using von Mises stresses under tensile loading, albeit with a smaller critical distance. Further investigation into the applicability of von Mises stress within the TCD framework under varying constraint conditions would be of interest to better understand the observed deviations.

The findings of this study are relatable to structural applications where localized stress raisers govern fatigue performance. For welded joints, the TCD has been extensively used to improve fatigue strength

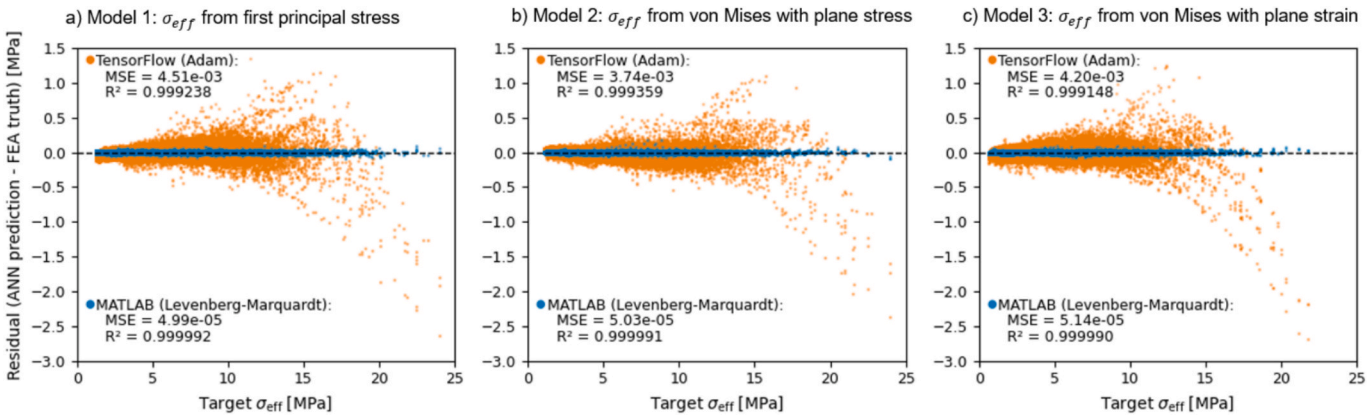

Fig. 12. Comparing test residuals for combined TCD methods between the Models trained with first-order Adam and second order Levenberg-Marquardt optimization algorithms.

predictions and to reduce scatter in experimental S-N curves through the consideration of local notch stresses [9–17]. In this work, the systematic variation of d, r and ω may be translatable to configurations found in fillet welds, butt-weld toes and undercuts when observed through idealized 2D cross sections perpendicular to the weld direction [61]. The observed differences in stability between PM, LM and AM regarding the effective stresses therefore provide a quantitative insight into which gradient method may be most suited (or conservative) for practical welded-joint assessment. Likewise, this approach may be further expanded to post-weld notch treatment such as high frequency impact treatment or TIG-dressing, where modifications to the local geometry are known to have a significant influence on fatigue behavior [13,14].

Recent studies have combined the TCD with high-fidelity surface digitalization methodologies such as laser scanning or structured-light profilometry in the analysis of notches for weld quality assessment [29,30,62,63]; however, the need to apply reverse engineering methodologies prior to FEA simulations results in a time- and computationally-expensive process to accurately determine the effective stresses. Shojai et al [30] argues that the TCD methods are of limited use when assessing samples that require the individual assessment of each individual notch—such as corroded specimens—due to the post-processing requirements. On the other hand, recent studies have introduced methodologies to automatically obtain 2D notch geometry parameters from surface scan results, see [63,64]. It should be noted however, different optical measurement methods as well as the spatial resolution of the surface scan may result in different characterization of such parameters, where further standardization work is needed [61]. The proposed workflow from this study can combine with such methodologies by applying the ANN-based metamodels to notch geometries obtained through an automated scan process with the applicable load case, as also proposed by Braun et al. [39]. This, in turn, can improve the efficiency of in-line quality assessment of notched components through a real time prediction of local effective stresses for fatigue assessment.

ANN based metamodels trained with FEA simulations have seen promising results in recent fatigue and fracture related studies [37–41,65]. In line with these studies, our work found that metamodels are able to significantly decrease the computational time needed compared to numerical simulations by numerous magnitudes. In terms of accuracy, R^2 values of > 0.99999 and average MSE values of $< 5 \times 10^{-5}$ were achieved for in line with the findings that neural networks are very well fitted to mechanical applications using FEA based datasets [37–41,43,65–67]. Despite this high predictive accuracy, ANNs are known for their limited interpretability, which motivates the comparison with surrogate models such as polynomial regression. Oswald et al. [37,38,41] also investigated polynomial regression with coupling terms as an alternative approach. This was also applied in this study; however, comparatively poor MSE results combined with the multiple target variables resulted in the method being an unsuitable alternative.

The second-order Levenberg–Marquardt optimizer was found to perform very effectively when training the individual metamodels. This aligns well with recent studies using second-order optimization based on deterministic FEA-based datasets [37–41,65]. In this work, Levenberg–Marquardt reliably achieved low residual errors and stable convergence behavior even when normally distributed scatter was added to the dataset, indicating that the underlying stress gradients are sufficiently smooth for second-order curvature information during training. In contrast, previous studies have favored training of mechanics-based surrogates using the first-order Adam optimizer [66,67]; however, Adam proved unable to produce competitive models in our work. This may be attributed to architectural differences, as the cited studies did not restrict their investigations to feedforward networks. An additional outcome of our hyperparameter tuning was that Levenberg-Marquardt converged on a markedly smaller and more compact network architecture compared to Adam, thereby reducing the computational cost of subsequent effective-stress predictions.

7. Conclusions

In this work, ANN based metamodels were trained to determine effective stress in notched flat bars based on the TCD methodology, using a range of notch geometrical parameters under varied loading conditions. This can simplify the process of estimating notch failure, through eliminating the need for FEA analysis and stress field integration for each individual notch geometry. Moreover, this study underlines the importance of carefully considering stress gradient methods, shown through the substantial deviations seen across the TCD based predictions across varied material characteristic lengths, notch geometries and load cases.

This study contributes to the understanding of effective stresses in notched flat bars combined with metamodeling through several main findings:

- Significant deviations were identified between the TCD variants, with peak differences of up to 40.4% for von Mises stresses and 24.2% for first principal stresses within the ranges evaluated in the parametric study. These discrepancies were strongly governed by notch radius, characteristic length L, loading mode, and plane state, underlining the need for careful method selection in fatigue and fracture assessments.
- Loading case and geometry both influenced deviation behavior, with sharp notches showing particularly high sensitivity at smaller L values and deviations that tended to converge as L increased under tension, whereas, deviations for bending loading tended to diverge with increasing L, especially for blunter notches.

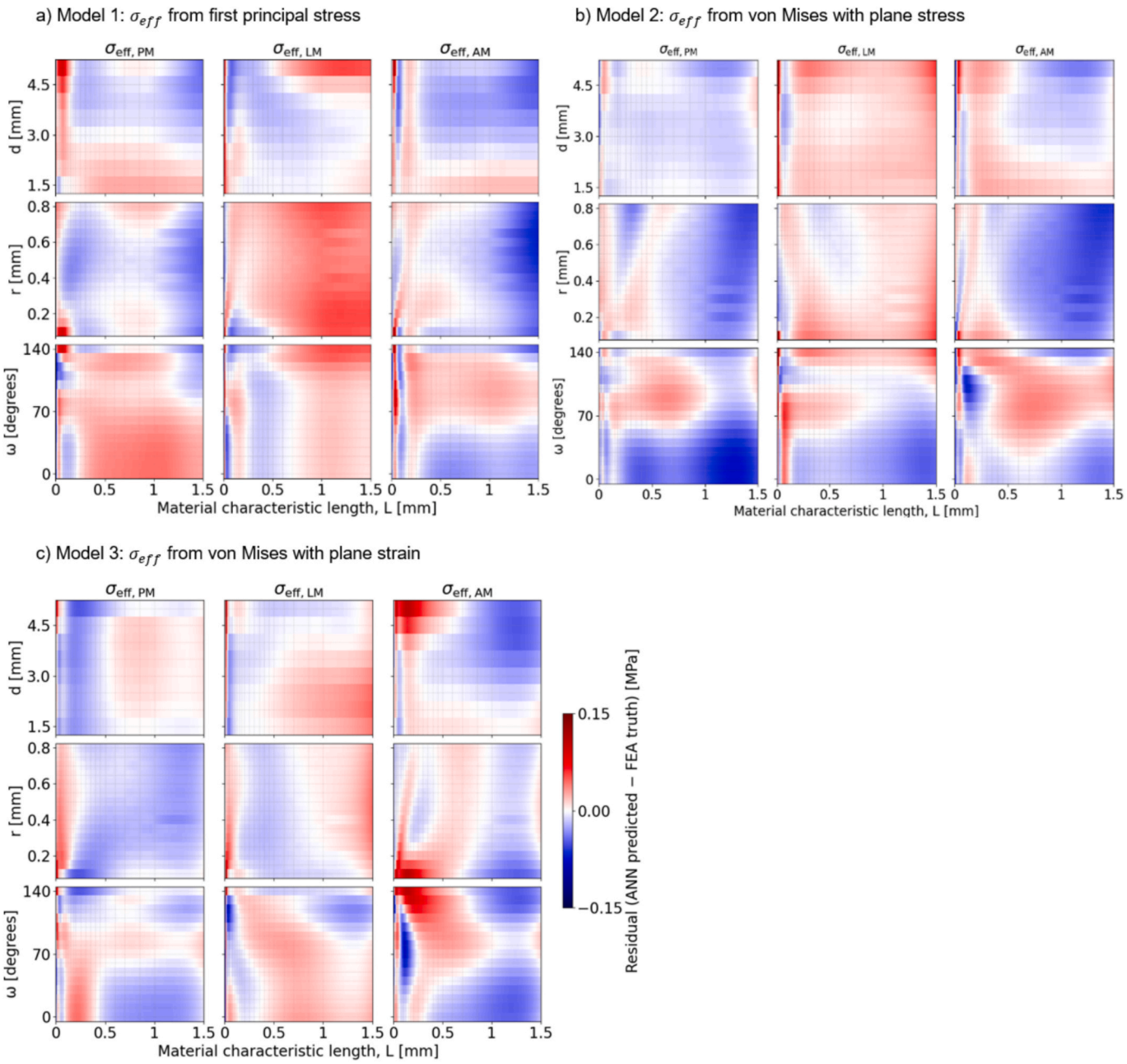

Fig. 13. Residual colormaps based on geometric parameters for the resulting three Levenberg-Marquardt-trained metamodels.

- The conversion-factor analysis showed that the usual relations $r_{PM} = \frac{L}{2}$ and $r_{LM} = 2L$ do not consistently align the TCD methods, with q varying strongly across geometries and load cases. Deviations were most pronounced at small L, under bending, and for von Mises plane-strain conditions, indicating that these ratios may be unsuitable for such scenarios.
- ANN-based metamodels demonstrated high predictive capability, achieving R^2 values of > 0.99999 and average MSE values of $< 5 \times 10^{-5}$, closely reproducing the effective-stress behavior of the FEA-based TCD calculations while reducing computational cost and increasing speed by many orders of magnitude.
- The Levenberg–Marquardt optimizer consistently outperformed first-order alternatives for the FEA-based dataset, yielding smaller, more efficient network architectures and more stable convergence. This highlights the importance of optimizer choice in mechanics-based surrogate modelling.
- The resulting ANN framework enables rapid effective stress prediction, eliminating the need for FEA and providing a foundation for real-time notch assessment when combined with automated scan-based geometry determination.

The trained ANN models are made freely available by the authors and can be readily fine-tuned with additional data. The underlying methodological framework—linking FEA-derived effective stresses with data-driven metamodeling—is transferable to more complex cross-sectional configurations, such as slices of welded joints. An important future step will be to broaden the training domain to include three-dimensional notch geometries, thereby further increasing the applicability to complex real-world structures.

In addition to the gradient methods encompassed by the TCD, approaches using control parameters such as strain energy density can be used to predict notch failure as summarized by Liao et al. [68]. Moreover, the implicit gradient method has seen promising results in notch

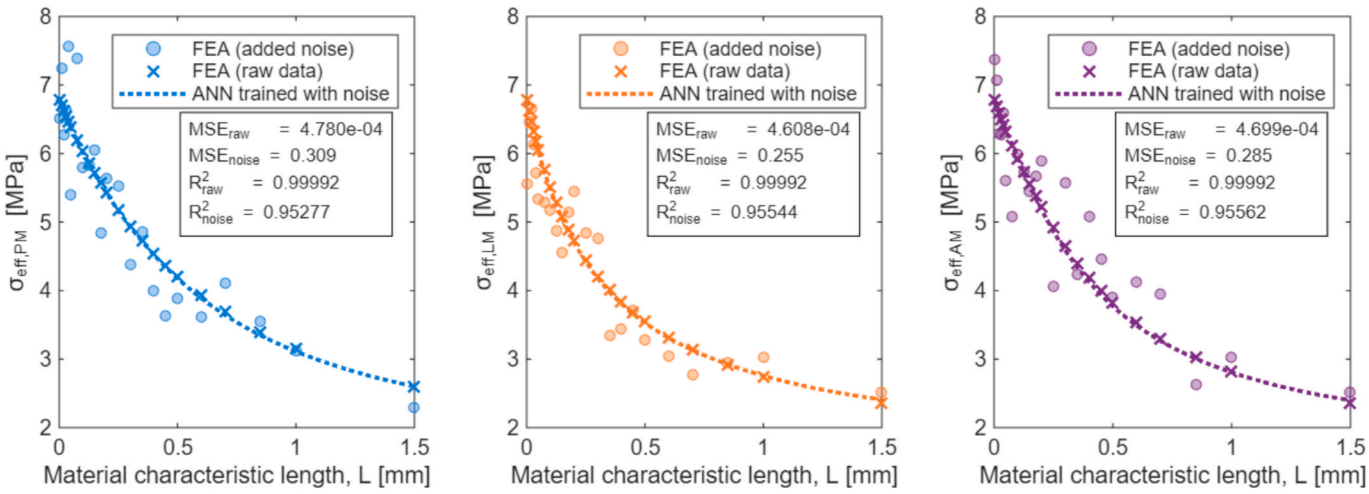

Fig. 14. *L* vs σ_{eff} for raw targets from FEA, targets with added noise, and results from ANN model retrained with added noise using Levenberg-Marquardt. Plotted here using a single notch subset for the three TCD methods.

failure of corroded specimens under cyclic loading [29,30]. Further studies could therefore include the results from additional notch failure prediction methods as target variables such as the volume method [2], implicit gradient method or control parameter-based approaches to expand the ANN-based prediction framework. Finally, including experimental fatigue results in the training dataset could correct systematic biases in the FEA-based predictions, enabling the metamodel to better reflect real-world behavior. Together, these steps outline clear pathways to extend the present modelling framework while preserving its efficiency and practicality for engineering applications.

CRediT authorship contribution statement

Kane F. ter Veer: Software, Methodology, Data curation, Writing – original draft, Visualization, Formal analysis. **Mathis Harder:** Writing – review & editing, Validation, Software, Methodology, Data curation. **Kagan Koyunseven:** Writing – original draft, Visualization, Software, Investigation, Formal analysis, Data curation. **Sascha M. Isay:** Validation, Writing – review & editing, Supervision. **Moritz Braun:** Writing – review & editing, Supervision, Resources, Project administration, Methodology, Conceptualization.

Declaration of competing interest

The authors declare that they have no known competing financial interests or personal relationships that could have appeared to influence the work reported in this paper.

Data availability

The metamodels and underlying datasets developed and used in this study are made freely available by the authors at https://data.mendeley.com/datasets/98v85vrhvr/12.

References

[1] Neuber H. Kerbspannungslehre: Grundlagen Für Genaue Festigkeitsberechnung Mit Berücksichtigung Von Konstruktionsform und Werkstoff. 2nd ed. Berlin, Heidelberg: Springer, Berlin / Heidelberg; 1958.
[2] Taylor D. The theory of critical distances: a new perspective in fracture mechanics, 1st ed. Oxford: Elsevier; 2007. [Online]. Available: https://www.sciencedirect.com/science/article/pii/s0013794407002172.
[3] Madrazo V, Cicero S, Carrascal IA. On the point method and the line method notch effect predictions in Al7075-T651. Eng Fract Mech 2012;79:363–79. https://doi.org/10.1016/j.engfracmech.2011.11.017.
[4] Hu Z, Berto F, Hong Y, Susmel L. Comparison of TCD and SED methods in fatigue lifetime assessment. Int J Fatigue 2019;123:105–34. https://doi.org/10.1016/j.ijfatigue.2019.02.009.
[5] Vedernikova A, Kostina A, Plekhov O, Bragov A. On the use of the critical distance concept to estimate tensile strength of notched components under dynamic loading and physical explanation theory. Theor Appl Fract Mech 2019;103:102280. https://doi.org/10.1016/j.tafmec.2019.102280.
[6] Atzori B, Campagnolo A, Ricotta M, Meneghetti G. Critical distances approach reformulated for a better comparison of fatigue strength of materials with sharp notches. Mat Design & Process Comms, 2(6); 2020: doi: 10.1002/mdp2.131.
[7] Benedetti M, Santus C, Fontanari V, Lusuardi D, Zanini F, Carmignato S. Plain and notch fatigue strength of thick-walled ductile cast iron EN-GJS-600-3: a double-notch critical distance approach to defect sensitivity. Int J Fatigue 2021;152:106414. https://doi.org/10.1016/j.ijfatigue.2021.106414.
[8] Shen X, Zeng D, Lu L. Investigating the effect of notch size on critical distance and fatigue limit by coupling the theory of critical distance and finite fracture mechanics. Theor Appl Fract Mech 2022;122:103566. https://doi.org/10.1016/j.tafmec.2022.103566.
[9] Susmel L. Four stress analysis strategies to use the modified Wöhler curve method to perform the fatigue assessment of weldments subjected to constant and variable amplitude multiaxial fatigue loading. Int J Fatigue 2014;67:38–54. https://doi.org/10.1016/j.ijfatigue.2013.12.001.
[10] Baumgartner J, Schmidt H, Ince E, Melz T, Dilger K. Fatigue assessment of welded joints using stress averaging and critical distance approaches. Weld World 2015;59(5):731–42. https://doi.org/10.1007/s40194-015-0248-x.
[11] Marulo G, Baumgartner J, Frendo F. Fatigue strength assessment of laser welded thin-walled joints made of mild and high strength steel. Int J Fatigue 2017;96:142–51. https://doi.org/10.1016/j.ijfatigue.2016.11.016.
[12] Karakaş Ö, Zhang G, Sonsino CM. Critical distance approach for the fatigue strength assessment of magnesium welded joints in contrast to Neuber's effective stress method. Int J Fatigue 2018;112:21–35. https://doi.org/10.1016/j.ijfatigue.2018.03.004.
[13] Baumgartner J, Yıldırım HC, Barsoum Z. Fatigue strength assessment of TIG-dressed welded steel joints by local approaches. Int J Fatigue 2019;126:72–8. https://doi.org/10.1016/j.ijfatigue.2019.04.038.
[14] Karakaş Ö, Leitner M, Tüzün N. Application of critical distance approach for fatigue assessment of welded and HFMI-treated steel joints. Int J Fatigue 2022;154:106534. https://doi.org/10.1016/j.ijfatigue.2021.106534.
[15] Braun M, Ahola A, Milaković A-S, Ehlers S. Comparison of local fatigue assessment methods for high-quality butt-welded joints made of high-strength steel. Forces Mech 2022;6:100056. https://doi.org/10.1016/j.finmec.2021.100056.
[16] Braun M, Milaković A-S, Ehlers S. Fatigue assessment of welded joints at sub-zero temperatures by means of stress averaging approach. Ships Offshore Struct 2021;16(sup1):216–24. https://doi.org/10.1080/17445302.2021.1906194.
[17] Taylor D, Hoey D. High cycle fatigue of welded joints: the TCD experience. Int J Fatigue, 31(10), pp. 20–27, 2009. [Online]. Available: https://www.sciencedirect.com/science/article/pii/s0142112308000194.
[18] Schmidt H, Baumgartner J, Melz T. Fatigue assessment of joints using the local stress field. Materialwissenschaft Werkst 2015;46(2):145–55. https://doi.org/10.1002/mawe.201400369.
[19] Beber VC, Schneider B, Brede M. Efficient critical distance approach to predict the fatigue lifetime of structural adhesive joints. Eng Fract Mech 2019;214:365–77. https://doi.org/10.1016/j.engfracmech.2019.03.022.
[20] Sousa FC, Akhavan-Safar A, Goyal R, Da Silva L. Fatigue life estimation of single lap adhesive joints using a critical distance criterion: an equivalent notch approach. Mech Mater 2021;153:103670. https://doi.org/10.1016/j.mechmat.2020.103670.

[21] Justo J, Castro J, Cicero S. Notch effect and fracture load predictions of rock beams at different temperatures using the theory of critical distances. Int J Rock Mech Min Sci 2020;125:104161. https://doi.org/10.1016/j.ijrmms.2019.104161.

[22] Aligholi S, Ponson L, Torabi AR, Zhang QB. A new methodology inspired from the theory of critical distances for determination of inherent tensile strength and fracture toughness of rock materials. Int J Rock Mech Min Sci 2022;152:105073. https://doi.org/10.1016/j.ijrmms.2022.105073.

[23] Benedetti M, Santus C. Notch fatigue and crack growth resistance of Ti-6Al-4V ELI additively manufactured via selective laser melting: a critical distance approach to defect sensitivity. Int J Fatigue 2019;121:281–92. https://doi.org/10.1016/j.ijfatigue.2018.12.020.

[24] Schnabel K, Baumgartner J, Möller B, Scurria M. Fatigue assessment of additively manufactured AlSi10Mg structures using effective stress concepts based on the critical distance approach. Weld World 2021;65(11):2119–33. https://doi.org/10.1007/s40194-021-01153-9.

[25] Lipiäinen K, Ahola A, Kaijalainen A, Björk T. Fatigue performance of notched and hot-dip galvanized laser and mechanically cut S960 steel components considering local defects with the theory of critical distances. Int J Fatigue 2022;164:107127. https://doi.org/10.1016/j.ijfatigue.2022.107127.

[26] Hao R, Lehto P, Lin W. Critical distance-based fatigue life evaluation of blunt notch details in steel bridges. J Constr Steel Res 2023;201:107738. https://doi.org/10.1016/j.jcsr.2022.107738.

[27] Sobotka JC, Enright MP, McClung RC. Application of critical distances to fatigue at pores. Fatigue Fract Eng Mat Struct 2019;42(8):1646–61. https://doi.org/10.1111/ffe.13004.

[28] Härkegård G. Critical-distance fatigue analysis of limiting cases of ellipsoidal cavities. Eng Fract Mech 2021;257:108011. https://doi.org/10.1016/j.engfracmech.2021.108011.

[29] Shojai S, Schaumann P, Ghafoori E. Micro-support effect consideration in fatigue analysis of corroded steel based on real surface geometry. J Constr Steel Res 2024;212:108259. https://doi.org/10.1016/j.jcsr.2023.108259.

[30] Shojai S, Brömer T, Ghafoori E, Schaumann P. Application of local fatigue approaches on corroded welded joints with consideration of weld geometry and residual stresses. Theor Appl Fract Mech 2024;129:104215. https://doi.org/10.1016/j.tafmec.2023.104215.

[31] Härkegård G, Halleraker G. Assessment of methods for prediction of notch and size effects at the fatigue limit based on test data by Böhm and Magin. Int J Fatigue 2010;32(10):1701–9. https://doi.org/10.1016/j.ijfatigue.2010.03.011.

[32] Radaj D, Sonsino CM, Fricke W. Fatigue assessment of welded joints by local approaches. 2nd ed. Cambridge, England: Woodhead; 2006.

[33] Santus C, Taylor D, Benedetti M. Experimental determination and sensitivity analysis of the fatigue critical distance obtained with rounded V-notched specimens. Int J Fatigue 2018;113:113–25. https://doi.org/10.1016/j.ijfatigue.2018.03.037.

[34] Susmel L, Taylor D. A novel formulation of the theory of critical distances to estimate lifetime of notched components in the medium-cycle fatigue regime. Fatigue Fract Eng Mat Struct 2007;30(7):567–81. https://doi.org/10.1111/j.1460-2695.2007.01122.x.

[35] Louks R, Susmel L. The linear-elastic theory of critical distances to estimate high-cycle fatigue strength of notched metallic materials at elevated temperatures. Fatigue Fract Eng Mat Struct 2015;38(6):629–40. https://doi.org/10.1111/ffe.12273.

[36] Braun M, Müller AM, Milaković A-S, Fricke W, Ehlers S. Requirements for stress gradient-based fatigue assessment of notched structures according to theory of critical distance. Fatigue Fract Eng Mat Struct 2020;43(7):1541–54. https://doi.org/10.1111/ffe.13232.

[37] Oswald M, Mayr C, Rother K. "Determination of notch factors for welded cruciform joints based on numerical analysis and metamodeling," (in En;en). Weld World 2019;63(5):1339–54. https://doi.org/10.1007/s40194-019-00751-y.

[38] Oswald M, Neuhäusler J, Rother K. Determination of notch factors for welded butt joints based on numerical analysis and metamodeling. Weld World 2020;64(12):2053–74. https://doi.org/10.1007/s40194-020-00982-4.

[39] Braun M, et al. Statistical characterization of stress concentrations along butt joint weld seams using deep neural networks. Appl Sci 2022;12(12):6089. https://doi.org/10.3390/app12126089.

[40] Neuhäusler J, Rother K. "Determination of notch factors for transverse non-load carrying stiffeners based on numerical analysis and metamodeling," (in En;en). Weld World 2022;66(4):753–66. https://doi.org/10.1007/s40194-021-01240-x.

[41] Oswald M, Neuhäusler J, Frey M, Rother K. "Determination of notch factors for welded T-joints based on numerical analysis and metamodeling," (in En;en). Weld World 2022;66(12):2609–24. https://doi.org/10.1007/s40194-022-01368-4.

[42] Chen C-H, Lai J-P, Chang Y-M, Lai C-J, Pai P-F. A study of optimization in deep neural networks for regression. Electronics 2023;12(14):3071. https://doi.org/10.3390/electronics12143071.

[43] Hoffer JG, Geiger BC, Ofner P, Kern R. Mesh-free surrogate models for structural mechanic FEM simulation: a comparative study of approaches. Appl Sci 2021;11(20):9411. https://doi.org/10.3390/app11209411.

[44] Peterson RE. Notch sensitivity. Metal Fatigue, pp. 293–306, 1959. [Online]. Available: https://cir.nii.ac.jp/crid/1573668924078557952.

[45] Taylor D, Cornetti P, Pugno N. The fracture mechanics of finite crack extension. Eng Fract Mech 2005;72(7):1021–38. https://doi.org/10.1016/j.engfracmech.2004.07.001.

[46] Susmel L, Taylor D. The theory of critical distances as an alternative experimental strategy for the determination of KIc and ΔKth. Eng Fract Mech 2010;77(9):1492–501. https://doi.org/10.1016/j.engfracmech.2010.04.016.

[47] Berto F, Lazzarin P, Radaj D. Fictitious notch rounding concept applied to sharp V-notches: evaluation of the microstructural support factor for different failure hypotheses. Part I: Basic stress equations. Eng Fract Mech 2008;75(10):3060–72. https://doi.org/10.1016/j.engfracmech.2007.12.011.

[48] Yosibash Z, Priel E, Leguillon D. A failure criterion for brittle elastic materials under mixed-mode loading. Int J Fract 2006;141(1–2):291–312. https://doi.org/10.1007/s10704-006-0083-6.

[49] Meneghetti G, Lazzarin P. Significance of the elastic peak stress evaluated by FE analyses at the point of singularity of sharp V-notched components. Fatigue Fract Eng Mat Struct 2007;30(2):95–106. https://doi.org/10.1111/j.1460-2695.2006.01084.x.

[50] Zhang G, Sonsino CM, Sundermeier R. Method of effective stress for fatigue: Part II – applications to V-notches and seam welds. Int J Fatigue 2012;37:24–40. https://doi.org/10.1016/j.ijfatigue.2011.09.016.

[51] Lazzarin P, Campagnolo A, Berto F. A comparison among some recent energy- and stress-based criteria for the fracture assessment of sharp V-notched components under mode I loading. Theor Appl Fract Mech 2014;71:21–30. https://doi.org/10.1016/j.tafmec.2014.03.001.

[52] Ferro P, Peron M, Razavi S, Berto F, Torgersen J. The fatigue behavior of V-notches in presence of residual stresses: recent developments and future outcomes, 1971-8993, 11(42): 2017; 189–195, doi: 10.3221/IGF-ESIS.42.20.

[53] Schuscha M, Leitner M, Stoschka M, Meneghetti G. Local strain energy density approach to assess the fatigue strength of sharp and blunt V-notches in cast steel. Int J Fatigue 2020;132:105334. https://doi.org/10.1016/j.ijfatigue.2019.105334.

[54] Foti P, Ayatollahi MR, Berto F. Rapid strain energy density evaluation for V-notches under mode I loading conditions. Eng Fail Anal 2020;110:104361. https://doi.org/10.1016/j.engfailanal.2019.104361.

[55] ANSYS, mapdl API reference. [Online]. Available: https://mapdl.docs.pyansys.com/version/stable/api/index.html (accessed: Feb. 8 2024).

[56] Susmel L. The theory of critical distances: a review of its applications in fatigue. Eng Fract Mech 2008;75(7):1706–24. https://doi.org/10.1016/j.engfracmech.2006.12.004.

[57] Hornik K. Approximation capabilities of multilayer feedforward networks. Neural Netw 1991;4(2):251–7. https://doi.org/10.1016/0893-6080(91)90009-t.

[58] Wilamowski BM, Yu H. Improved computation for Levenberg-Marquardt training. IEEE Trans Neural Netw 2010;21(6):930–7. https://doi.org/10.1109/tnn.2010.2045657.

[59] Abdulkadirov R, Lyakhov P, Nagornov N. Survey of optimization algorithms in modern neural networks. Mathematics 2023;11(11):2466. https://doi.org/10.3390/math11112466.

[60] Susmel L, Taylor D. The theory of critical distances to estimate the static strength of notched samples of Al6082 loaded in combined tension and torsion. Part II: multiaxial static assessment. Eng Fract Mech 2010;77(3):470–8. https://doi.org/10.1016/j.engfracmech.2009.10.004.

[61] Schubnell J, et al. "Influence of the optical measurement technique and evaluation approach on the determination of local weld geometry parameters for different weld types," (in En;en). Weld World 2020;64(2):301–16. https://doi.org/10.1007/s40194-019-00830-0.

[62] Tanvir MH, Shojai S, Banaschik R, Braun M. Fatigue assessment of laser hybrid welded butt joints with severe imperfections using 3D scanning and critical distance theory. Weld World 2025. https://doi.org/10.1007/s40194-025-02189-x.

[63] Dänekas C, Schubnell J, Krautheimer J, Jung M, Ghafoori E, Schaumann P. Algorithms for determination of weld toe radius and weld toe angle in welded joints. J Constr Steel Res 2025;224:109112. https://doi.org/10.1016/j.jcsr.2024.109112.

[64] Heide KM, Heikebrügge S, Dänekas C, Breidenstein B, Schaumann P. "Automated geometry measurement and deep rolling of butt welds," (in En;en). Weld World 2022;66(12):2533–47. https://doi.org/10.1007/s40194-022-01346-w.

[65] Lu Z, Lai H, Zhou L, Shen Z, Ren X, Li X. Prediction of hydraulic fracture initiation pressure in a borehole based on a neural network model considering plastic critical distance. Eng Fract Mech 2022;274:108779. https://doi.org/10.1016/j.engfracmech.2022.108779.

[66] Lieu QX. A deep neural network-assisted metamodel for damage detection of trusses using incomplete time-series acceleration. Expert Syst Appl 2023;233:120967. https://doi.org/10.1016/j.eswa.2023.120967.

[67] Greve L, van de Weg BP. Surrogate modeling of parametrized finite element simulations with varying mesh topology using recurrent neural networks. Array 2022;14:100137. https://doi.org/10.1016/j.array.2022.100137.

[68] Liao D, Zhu S-P, Correia JA, de Jesus AM, Berto F. Recent advances on notch effects in metal fatigue: a review. Fatigue & Fract Eng Mater & Struct 2020;43(4):637–59. https://doi.org/10.1111/ffe.13195.